Numerical investigation of incompressible flow in grooved channels. Part 2. Resonance and oscillatory heat-transfer enhancement

By N. K. GHADDAR, M. MAGEN, B. B. MIKIC
AND A. T. PATERA

Department of Mechanical Engineering, Massachusetts Institute of Technology,
Cambridge, MA 02139, USA

Modulatory heat-transfer enhancement in grooved channels is investigated by direct numerical simulation of the Navier–Stokes and energy equations using the spectral element method. It is shown that oscillatory perturbation of the flow at the frequency of the least-stable mode of the linearized system results in subcritical resonant excitation and associated transport enhancement as the critical Reynolds number of the flow is approached. The Tollmien–Schlichting frequency theory that was presented in Part 1 of this paper is shown to accurately predict the optimal frequency for transport augmentation for small values of the modulatory amplitude, and the effect of the excited travelling-wave channel modes on the resulting temperature distribution is described. The importance of (non-trivial) geometry in the forced response of a flow is discussed, and grooved-channel flow is compared to (straight-channel) plane Poiseuille flow, for which no resonance excitation occurs owing to a zero projection of the forcing inhomogeneity on the dangerous modes of the system. For the particular grooved-channel geometry investigated, resonant oscillatory forcing at modulatory amplitudes as small as 20 % of the mean flow results in a doubling of transport as measured by a time, space-averaged Nusselt number.

1. Introduction

Heat transfer in grooved, furrowed, or finned-wall channels and ducts (Kern & Kraus 1972) plays a critical role in many important processes and devices, from industrial heat exchangers (Kays & London 1955) to the cooling of microscale electronic components (Arvizu & Moffat 1982; Ashiwake *et al.* 1983). In many of these applications, it is heat transfer mechanisms that limit the size, performance, and efficiency of the overall engineering systems, and it is therefore of great practical interest to determine ways in which to enhance grooved-channel heat transfer by appropriate modification of the environment (geometry, flow conditions) in which these controlling transport processes take place.

It has been found that oscillation of the driving flow is a promising approach to heat-transfer enhancement in grooved-wall systems, as was first isolated in a membrane blood oxygenator (Bellhouse *et al.* 1973), and subsequently confirmed by numerical (Sobey 1980, 1982, 1983; Ghaddar, Patera & Mikic 1984) and experimental (Stephanoff, Sobey & Bellhouse 1980) flow studies in a periodically furrowed channel. These investigations, for purely oscillatory flow at relatively low Reynolds number,

indicate that the interaction of separated flow with imposed unsteadiness leads to significant lateral convective motions, from which transport enhancement can then be inferred. However, no simple physical effect is implicated as being responsible for this strong effect of flow oscillation on separation, no doubt due to the order-unity interaction between these two phenomena for the zero-mean-flow case.

Of interest in the present study is the investigation of *modulatory* heat-transfer enhancement in grooved channels at 'moderate' Reynolds numbers ($0 < R < 1000$), in which the amplitude of the oscillatory perturbation η is typically no more than a small fraction of the mean flow. The motivation for this work derives from the findings of Part 1 of this paper (Ghaddar *et al.*, 1986, hereinafter referred to as I), in which it is shown that the least-stable linear mode of grooved-channel flow is oscillatory in nature, with a critical Reynolds number R_c on the order of 1000. These results concerning the unforced response of grooved-channel flow suggest that subsequent appropriately tuned oscillatory modulation should result in strong resonant response as $R \Rightarrow R_{c-}$, with a corresponding dramatic increase in the associated heat transfer.

This phenomenon of subcritical resonance and transport enhancement is the subject of the current paper, in which we investigate heat transfer in incompressible oscillatory flow in two-dimensional periodically grooved channels by direct numerical simulation of the Navier–Stokes and energy equations. The general subject area of the effect of oscillation on stability and flow behaviour is, of course, not new, and there has been much work in the past on destabilization by oscillation in homogeneous domains (see Davis 1976 for a review). Of interest here is examining the extent to which complex, *non*-homogeneous geometry affects the stability and response characteristics of oscillatory forced flows, and investigating the degree to which such flow behaviour can be exploited for purposes of transport augmentation.

In §2 we present the full problem formulation, and discuss the thermal boundary conditions imposed. In §3 we pose the forced linearized problem, and present formal solutions to the linear equations. The critical role played by geometry in oscillatory flows is demonstrated, and comparisons made between the cases of grooved and ungrooved channels. In §4 heat-transfer solutions are presented for the case of steady flow, thus providing a baseline from which to evaluate the effect of oscillatory forcing on transport. In §5 we present numerical solutions to the forced linearized equations, verifying the predictions of §3. The significant effect of resonance on heat-transfer enhancement is demonstrated. Lastly, in §6 we present the results of our full nonlinear calculations, and discuss the effects of nonlinearity on transport and the frequency selection process. The structure of the velocity and temperature fields is analysed, and a brief parametric study of the effect of Prandtl number and geometry is given.

2. Problem formulation

The geometry to be considered is the periodically grooved channel shown in figure 1 (identical to that in I), assumed infinite in extent in the streamwise (x) and spanwise (z) directions. The flow is assumed to be fully developed in x, and to be independent of spanwise coordinate z. The thermal boundary conditions are taken to be those of uniform flux on the bottom (grooved) wall ∂D_B, with an adiabatic top surface ∂D_T. Natural convection, variation of thermal properties, and non-fully developed effects are all assumed to be negligible.
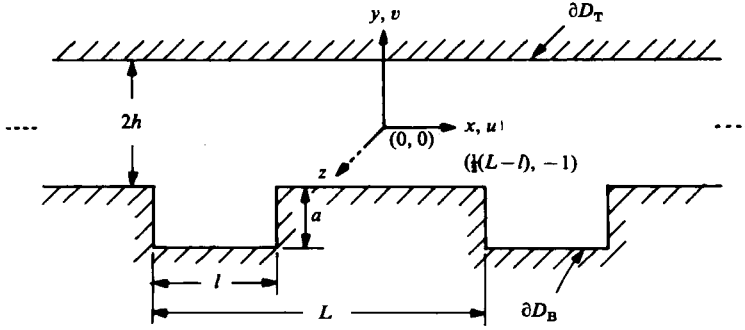
FIGURE 1. The geometry of the periodically grooved channel is described by the groove depth a, the groove length l, and the separation distance between the grooves L, all non-dimensionalized with respect to the channel half-width h. The geometry is assumed infinite in the streamwise (x) and spanwise (z) directions.

To put the problem in non-dimensional form, we scale all velocities by $\frac{3}{2}V$, where V is the time-mean cross-channel average velocity,

$$V = (2h)^{-1} \int_{-h}^{h} \langle u(x = 0, y, t) \rangle \, \mathrm{d}y,$$

with brackets referring to temporal average. Length is non-dimensionalized by the channel half-width h and temperature by $q''h/k$, where q'' is the uniform flux imposed at the bottom wall, and k is the thermal conductivity of the fluid. (Hereinafter all variables are assumed to be non-dimensional unless otherwise indicated.) This gives the following equations for the velocity $v(x,t)$ $(= u\hat{x} + v\hat{y})$, and the temperature $T(x,t)$:

$$v_t = v \times \omega - \nabla \Pi + R^{-1}\nabla^2 v, \quad \text{in } D \tag{1a}$$

$$\nabla \cdot v = 0, \quad \text{in } D, \tag{1b}$$

and
$$T_t + \nabla \cdot (vT) = (R\,Pr)^{-1}\nabla^2 T \quad \text{in } D, \tag{2}$$

respectively, where the domain D is defined by the periodicity length between grooves L, the length of the grooves l, and the depth of the grooves a. Here Π is the dynamic pressure, ω is the vorticity, $\omega = \nabla \times v$, $R = \frac{3}{2}Vh/\nu$ is the Reynolds number, and Pr is the Prandtl number, $Pr = \nu/\alpha$, where ν and α are the kinematic viscosity and thermal diffusivity respectively. Most results presented in this paper are for the 'base' geometry given in I, corresponding to $L = 6.6666$, $l = 2.2222$, $a = 1.1111$.

The fully developed boundary conditions for the velocity $v(x,t)$ are as in I:

$$v(x,t) = 0, \quad \text{on } \partial D \tag{3a}$$

$$v(x+mL, y, t) = v(x, y, t), \tag{3b}$$

with L the periodicity length between grooves, and m the integer periodicity index. For the pressure we require

$$\Pi(x,t) = -f(t)\,x + \tilde{\Pi}(x,t), \tag{4a}$$

$$\tilde{\Pi}(x+mL, y, t) = \tilde{\Pi}(x, y, t), \tag{4b}$$

where the term $f(t)$ is the driving force for the flow, and is determined (indirectly) by the imposed flow-rate condition

$$Q = \int_{\partial D_B}^{\partial D_T} u(x,y,t)\,dy = \tfrac{4}{3}(1 + \eta \sin 2\pi\Omega_F t) \tag{5}$$

(independent of x). Here η is the amplitude of the modulatory component of the flow (the results in I correspond to $\eta = 0$), and Ω_F is the Strouhal number of the forced oscillation.

For the temperature boundary conditions on the top and bottom walls we have

$$\nabla T \cdot \hat{n} = 1 \quad \text{on } \partial D_B, \tag{6a}$$

$$\nabla T \cdot \hat{n} = 0 \quad \text{on } \partial D_T \tag{6b}$$

respectively, where $\hat{n}$ refers to the outward normal on the domain boundary. As regards the condition that the flow is fully developed, we cannot simply impose periodicity of $T(x,t)$, as this is inconsistent with the boundary conditions (3) and (6) if steady or steady-periodic solutions are sought. Rather, we must first subtract a linear term to compensate for the rise in mixed-mean temperature along the channel due to the net flux input (6), giving as the appropriate periodicity condition

$$T(x,t) = \theta(x,t) + \frac{3}{4}\left(1 + \frac{2a}{L}\right)\frac{x}{R\,Pr}, \tag{7a}$$

$$\theta(x + mL, y, t) = \theta(x, y, t). \tag{7b}$$

These boundary conditions can be shown to result in a consistent (solvable) set of equations for determination of the temperature in the cases of steady or steady-periodic flow, as is readily demonstrated by integration of (2) over the flow domain, use of conditions (3), (5) and (6), and averaging in time. The details of this simple demonstration, as well as a discussion of the physical relevance of the fully developed boundary conditions, (7), are given in Ghaddar, Karniadakis & Patera (1986). We have used the flux boundary conditions, (6), rather than the simpler case of isothermal walls, as the former are often a better model for practical applications and experimental configurations. Our results are not qualitatively sensitive to the particular thermal boundary conditions chosen.

3. Linear theory – formal solution

In addition to the fully nonlinear problem (1)–(7), we shall also consider the linear problem in which we perturb the flow in an oscillatory fashion about a known (stable) steady state. This will allow us to interpret our results in the context of the previous work on unforced flow (see I), as well as subsequently determine the effect of nonlinearity on the resonance phenomenon. To arrive at the forced linear problem, we do a perturbation expansion for the velocity in the forcing parameter η,

$$v(x,t) = v_s(x) + \eta v'(x,t) \quad (\eta \ll 1), \tag{8}$$

where v_s is the (numerically obtained) steady solution to the grooved-channel problem (see I). Inserting (8) into (1) and neglecting terms $O(\eta^2)$ and higher then gives the following linear equation for $v'(x,t)$:

$$v'_t = v_s \times \omega' + v' \times \omega_s - \nabla \tilde{\Pi}' + f'\hat{x} + R^{-1}\nabla^2 v', \tag{9a}$$

$$\nabla \cdot v' = 0. \tag{9b}$$

The boundary conditions on v', Π' are as for the nonlinear problem, (3)–(4), however the flow-rate condition (5) is now replaced with

$$Q'(t) = \int_{\partial D_B}^{\partial D_T} u'(x, y, t)\,\mathrm{d}y = \tfrac{4}{3}\sin 2\pi\Omega_F t. \tag{10}$$

Once we have determined the velocity from (8)–(10), we solve the full passive scalar equation (2),

$$T_t + \boldsymbol{\nabla}\cdot[(v_s + \eta v')\,T] = (R\,Pr)^{-1}\nabla^2 T, \tag{11}$$

for the temperature, with boundary conditions (6)–(7) as before. As the motivation behind (8) is linearization, and not perturbation *per se*, we have kept terms to all orders of η in (11). This will be discussed further in §5.

In §5, we shall solve (9)–(11) by direct numerical simulation and discuss the frequency, Reynolds-number and amplitude (η) dependence of the linear response. To motivate these results, and also highlight the critical role of geometry in resonance, we present here a formal analytical solution to the linear problem. To begin, we redefine (9) in terms of a stream-function representation, defining the velocity as

$$\boldsymbol{v}'(\boldsymbol{x}, t) = \boldsymbol{\nabla} \times \psi(x, y, t)\,\hat{\boldsymbol{z}}, \tag{12}$$

and writing (9) as

$$\mathscr{L}\psi = \mathrm{M}\psi_t, \tag{13}$$

with boundary conditions

$$\boldsymbol{\nabla}\psi\cdot\hat{\boldsymbol{n}} = 0 \quad \text{on } \partial D, \tag{14a}$$

$$\psi = 0 \quad \text{on } \partial D_B, \tag{14b}$$

$$\psi = Q'(t) \quad \text{on } \partial D_T. \tag{14c}$$

Here the operators $\mathscr{L}$ and M are defined as

$$\mathscr{L}\psi = -\nabla^4\psi + J(\nabla^2\psi_s, \psi) - J(\psi_s, \nabla^2\psi), \tag{15a}$$

$$\mathrm{M}\psi = -\nabla^2\psi, \tag{15b}$$

where ψ_s is the steady-state stream function, $\boldsymbol{v}_s = \boldsymbol{\nabla} \times \psi_s\,\hat{\boldsymbol{z}}$, and $J(u, v)$ is the Jacobian operator defined as $J(u, v) = u_x v_y - u_y v_x$.

Although the two formulations (9) and (13) are, by construction, equivalent, we see that the flow-rate condition enters directly into (13) as a boundary condition, (14c), whereas in (9) it is a constraint imposed by the pressure gradient term, $f'(t)$. This pressure gradient term, $f'(t)$, which can be thought of as part of the *response* of the system, does not appear in the stream-function equations explicitly (as it is irrotational), however it can be recovered by integration of the x-component of (9a) along the top boundary ∂D_T,

$$f'(t) = -(RL)^{-1}\int_0^L u'_{yy}\,\mathrm{d}x|_{\partial D_T} = -(RL)^{-1}\int_0^L \psi_{yyy}\,\mathrm{d}x|_{\partial D_T}. \tag{16}$$

This term will be instrumental later in determining whether or not resonance obtains.

Continuing with our formal solution of (13) and (14), we adopt the usual procedure of expanding ψ in terms of the eigenfunctions $\psi_k(x, y)$ of the homogeneous problem associated with (13)–(14),

$$\mathscr{L}\psi_k = s_k\mathrm{M}\psi_k \quad \text{in } D, \tag{17}$$

$$\boldsymbol{\nabla}\psi_k\cdot\hat{\boldsymbol{n}} = 0 \quad \text{on } \partial D, \tag{18a}$$

$$\psi_k = 0 \quad \text{on } \partial D, \tag{18b}$$

with corresponding adjoint problem

$$\mathcal{L}^* \psi_k^* = \bar{s}_k \mathrm{M}^* \psi_k^* \quad \text{in } D, \tag{19}$$

$$\nabla \psi_k^* \cdot \hat{n} = 0 \quad \text{on } \partial D, \tag{20a}$$

$$\psi_k^* = 0 \quad \text{on } \partial D. \tag{20b}$$

The adjoint operators $\mathcal{L}^*$, M^*, are given by

$$\mathcal{L}^* \psi^* = -\nabla^4 \psi^* - J(\nabla^2 \psi_s, \psi^*) + \nabla^2 J(\psi_s, \psi^*), \tag{21a}$$

$$\mathrm{M}^* = \mathrm{M}, \tag{21b}$$

for which, by construction, $(u, \mathcal{L}v) = (\mathcal{L}^*u, v)$, $(u, \mathrm{M}v) = (\mathrm{M}^*u, v)$, for u, v satisfying the homogeneous boundary conditions (18). Here (u, v) is the usual scalar product

$$(u, v) = \iint_D \bar{u}v \, \mathrm{d}\boldsymbol{x}, \tag{22}$$

where overbar denotes complex-conjugate.

We now assume completeness in the sense that, for a function $g(\boldsymbol{x})$ which satisfies all of the boundary conditions (18), the expansion

$$g(\boldsymbol{x}) = \sum_{k=1}^{\infty} a_k \psi_k(\boldsymbol{x}), \tag{23a}$$

$$a_k = (\psi_k^*, \mathrm{M}g), \tag{23b}$$

converges sufficiently fast so as to allow termwise evaluation of $\mathcal{L}g$. The coefficients (23b) follow from the usual orthogonality conditions

$$(\psi_m^*, \mathrm{M}\psi_n) = \delta_{mn}, \tag{24a}$$

$$(\psi_m^*, \mathcal{L}\psi_n) = s_n \delta_{mn}. \tag{24b}$$

Although we have no proof of the above claims for arbitrary geometry, these results have been shown to be true for the case of a plane channel (Diprima & Habetler 1969), and seem plausible for the case considered here.

If we now consider the forced problem (13)–(14), it is clear that ψ will not satisfy the homogeneous boundary conditions (18), and thus the validity of the expansion (23) is no longer a reasonable assumption. To avoid this problem, we write

$$\psi(x, y, t) = \phi(x, y, t) + \tilde{\phi}(x, y, t), \tag{25a}$$

$$\tilde{\phi}(x, y, t) = \tfrac{3}{4}Q'(t)\,\psi_s(x, y), \tag{25b}$$

where it is seen that ϕ now does satisfy the conditions (18), and is therefore expandable according to (23). (Note the choice of $\tilde{\phi}$ is clearly not unique, as any function incorporating the inhomogeneous boundary conditions (14c) will suffice.) Inserting (25) and (10) into (13)–(14), we obtain the following equation for ϕ:

$$\mathcal{L}\phi - \mathrm{M}\phi_t = -(\mathcal{L} - \mathrm{i}\omega_F \mathrm{M})\psi_s \exp(\mathrm{i}\omega_F t), \tag{26}$$

with associated homogeneous boundary conditions, (18). Here $\omega_F = 2\pi\Omega_F$, and, consistent with (10), we take the imaginary part of ϕ to be our physical solution.

Of interest here is understanding under what conditions (26) admits resonant solutions, that is solutions which exhibit secular (non-periodic) behaviour in time. Such solutions will clearly characterize the response of the flow to oscillatory forcing,

even at subcritical Reynolds numbers. We begin by assuming time-asymptotic solutions of the form

$$\phi(x, y, t) = \phi'(x, y) \exp(i\omega_F t), \tag{27}$$

corresponding to periodic behaviour in time; if solutions of the form (27) can be found, resonance will not occur, whereas if (27) leads to a non-solvable system, resonance will obtain. Inserting (27) in (26) gives the (purely spatial) problem for ϕ',

$$(\mathscr{L} - i\omega_F M)\phi' = -(\mathscr{L} - i\omega_F M)\psi_s. \tag{28}$$

We then expand ϕ' as in (23a),

$$\phi'(x, y) = \sum_{k=1}^{\infty} a_k \psi_k(x), \tag{29}$$

insert (29) into (28), and use orthogonality, (24), to arrive at the following equation for the modal amplitudes a_k:

$$(s_k - i\omega_F) a_k = -\iint_D \overline{\psi}_k^*(\mathscr{L} - i\omega_F M)\psi_s \, dx. \tag{30a}$$

Integration by parts can be used to further simplify the right-hand side of (30a), giving

$$(s_k - i\omega_F) a_k = \tfrac{4}{3}L\overline{f}_k'^* - (s_k - i\omega_F)(\psi_k^*, M\psi_s), \tag{30b}$$

where $f_k'^*$ is the modal adjoint pressure gradient term

$$f_k'^* = -(RL)^{-1} \int_0^L (\psi_k^*)_{yyy} \, dx|_{\partial D_T}, \tag{31}$$

analogous to (16).

Looking at (30b), we can now clearly state the conditions for resonance. First, the flow must become unstable at some critical Reynolds number R_c defined by the zero-crossing of σ_1. Secondly, the unstable mode must be oscillatory in nature, that is Ω_1 must be non-zero. Resonance will then occur as $\Omega_F \Rightarrow \Omega_1$, $R \Rightarrow R_c$, *as long as the right-hand side of* (30b) *remains non-zero in this limit.* If the first two conditions are satisfied, the last constraint can be seen to be equivalent to the requirement

$$f_1'^* \neq 0, \tag{32}$$

that is that the forcing term have a non-zero projection on the critical mode. We can also state the resonance conditions in terms of (28), in which it is seen that resonance will occur when the left-hand-side operator becomes singular, and the equation non-solvable (that is when the right-hand side is not orthogonal to $\overline{\psi}_1^*$). Equation (30b) also suggests the possibility of secondary peaks (i.e. local maxima in the frequency response) corresponding to excitation of higher modes (Ω_k, $k \geqslant 2$) of the linear system.

In the case of resonance, $R = R_c$, $\Omega_F = \Omega_1$, $f_1'^* \neq 0$, the expansion (27) and all that follows is no longer appropriate, and we must use instead

$$\phi = \exp(i\omega_F t)(ta_1'\psi_1(x, y) + \phi'), \tag{33}$$

with ϕ' expanded as before in (29). Inserting (33) into (26) then gives the following equation for ϕ':

$$(\mathscr{L} - i\omega_F M)\phi' = a_1' M\psi_1 - (\mathscr{L} - i\omega_F M)\psi_s. \tag{34a}$$

Although (34a) is still singular, the proper choice of a_1',

$$a_1' = -\tfrac{4}{3}L\overline{f}_1'^*, \tag{34b}$$

results in a solvable equation, as can be easily seen by inspection of (34a) and (30b). The fact that the solution (33) is unbounded as $t \Rightarrow \infty$ is, of course, non-physical, an indication that nonlinear effects will quickly intervene. However, (33) is nevertheless evidence that, as $R \Rightarrow R_c$, the flow will respond to appropriately tuned forcing with large-amplitude fluctuations and associated transport enhancement.

The formal conditions for resonance given above are, in fact, only a particular case of a general theory described in Magen & Patera (1986). This more general theory proceeds by considering dual eigenproblems: the first eigenproblem corresponds to imposed (zero) flow rate $Q' = 0$, in which the pressure drop f' is taken as part of the homogeneous response of the system (this is the formulation considered in I, as well as in (17) and (18) of the current paper); the second eigenproblem corresponds to (zero) imposed pressure drop $f' = 0$, with the resulting flow rate, Q', now interpreted as part of the internal system response. It can then be shown that resonance occurs only in flows for which the critical mode is *not* common to both eigenproblems. Interpreting our result (32) in terms of these arguments, we see that resonance occurs for our imposed flow-rate system only if the pressure drop of the critical mode of the corresponding homogeneous problem is non-zero. Physically, the inhomogeneity $\frac{4}{3}L\bar{f}_k'^*$ in (30b) is the product of the oscillatory flow-rate magnitude and the resulting modal pressure drop; this is equivalent to the power input into the system, and is therefore a measure of the oscillatory susceptibility of the flow.

It might appear that the subcritical resonance phenomenon described here is a rather trivial exploitation of the natural modes of a continuous system, and, in some sense, this is true. However, there are some subtle complications that explain why the phenomenon has not been widely studied or exploited. First, there is the rather obvious requirement that Ω_1 be non-zero; for many of the geometries and physical problems that are analytically tractable (e.g. Bénard convection between parallel plates, Taylor–Couette flow between concentric cylinders), translation invariance and geometric homogeneity result in exchange of stability, and therefore the linear resonance phenomenon no longer obtains.

The second, more interesting, requirement for resonance is (32), namely that the adjoint forcing term be non-zero in order that (28) be non-solvable. We illustrate the significant effect of geometry on satisfaction of this constraint by first considering the case of plane Poiseuille flow ($a = 0$ in figure 1), for which (17) and (18) reduce to the classical Orr–Sommerfeld equation (see I, also Drazin & Reid 1981), with the ψ_k now corresponding to Tollmien–Schlichting waves characterized by wavenumbers $\alpha_m = 2\pi m/L$. It is clear that for $\alpha_m \neq 0$, $f_k'^* = 0$, as in this case, the integration in (31) corresponds to the average of a non-zero Fourier mode. The only possible resonance modes must therefore correspond to $\alpha_m = 0$; however, as these (Stokes) modes are purely decaying, we conclude that linear subcritical resonance can not occur for plane Poiseuille flow. The only dangerous (Orr–Sommerfeld) modes of the system are solutions to both the imposed flow-rate and imposed pressure-drop eigenproblems, and the flow is therefore not susceptible to oscillatory perturbation.

In fact, within the context of our linearized (in η) theory, oscillation of plane Poiseuille flow results only in Womersley flow (Davis 1976), with no excitation of the 'non-trivial', unstable (Tollmien–Schlichting) modes of the system. Furthermore, there is no vertical velocity generated, and, hence, no transport enhancement. (For other thermal boundary conditions appropriate for the study of longitudinal transport, there may indeed be enhancement even in Womersley flow (Watson 1983; Joshi *et al.* 1983), however, our concern here is with lateral, resonant enhancement.) It should be noted that subcritical resonance is very different from oscillatory 'destabilization'
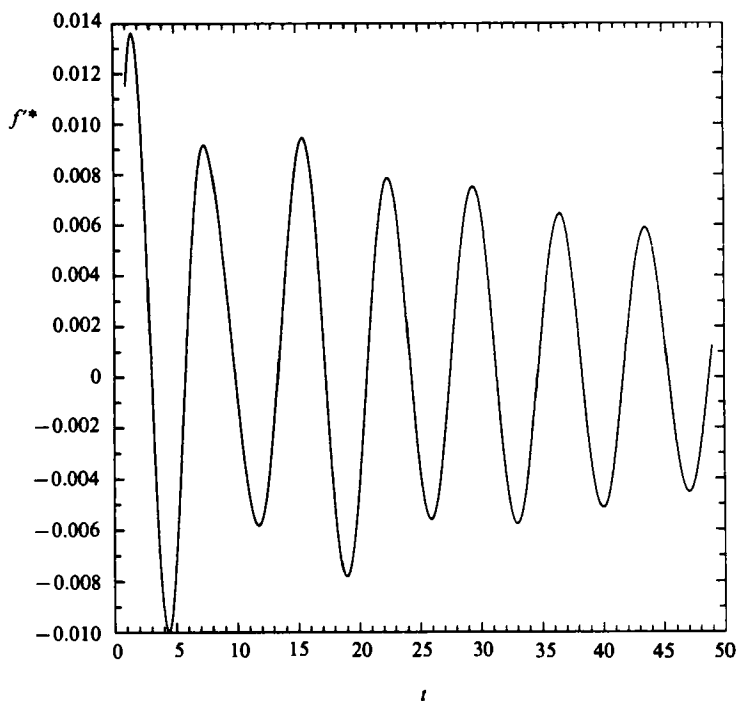
FIGURE 2. A plot of the adjoint forcing term f'^* for $R = 525$ and the base geometry, obtained by direct numerical simulation of the spectral element discretization of the unforced linear adjoint equation. The frequency of oscillation Ω_1, and the growth rate σ_1, of the time-asymptotic solution are the same as those found in I by consideration of the velocity field. The non-zero amplitude of the adjoint pressure term implies that resonance *will occur* in grooved channels.

such as parametric instability (Davis 1976; Drazin & Reid 1981), which, in the context of our small-η expansion, is a 'nonlinear' effect. The study of the stability of Womersley flow corresponds, in fact, to an investigation of the stability of the time-dependent flows *resulting* from solution of (9).

It is simple to (numerically) demonstrate that for *grooved*-channel flow this degeneracy as regards geometry disappears, and that the least-stable mode achieves a non-zero 'projection' on the adjoint forcing term $f_1'^*$. We plot in figure 2 $f'^*(t)$ obtained from direct numerical simulation of the spectral element discretization of the (time-dependent, primitive-variable) unforced linear adjoint equation, (19)–(21), at $R = 525$, for the base geometry $L = 6.6666$, $l = 2.2222$, $a = 1.1111$. (A detailed discussion of our direct simulation techniques for linear-theory calculations is given in I and the references therein.) The frequency and time-asymptotic decay rate from figure 2 are the same as those obtained in I by consideration of the velocity field, from which we conclude that the first (least-stable) mode of the grooved-channel flow corresponds to a non-zero adjoint pressure gradient term. It is shown in I that this oscillatory mode becomes unstable at $R_c = 975$, and thus grooved-channel flow satisfies all the requirements for resonance detailed above. The fact that resonance obtains implies that for the grooved channel (unlike the planar channel), the imposed flow-rate and imposed pressure-drop eigenproblems are not the same (Magen & Patera 1986); although in this series of papers we have considered only the flow-rate formulation, a complete analysis must include both.

Another way in which to see the singular difference between grooved and

ungrooved channels is to consider the nature of the instability modes. For plane Poiseuille flow, the Tollmien–Schlichting modes are travelling waves, and thus a Gallilean change of reference frame reduces the least-stable mode to a purely decaying one, for which we do not expect linear resonance. On the other hand, although the grooved-channel modes closely resemble travelling Tollmien–Schlichting waves in the channel region of the flow, the non-homogeneous geometry does *not* permit 'global' solutions of the form of travelling waves in the entire domain. Thus, just as the groove region perturbs the channel waves so as to destabilize them in the unforced problem, so it provides the mechanism by which the Tollmien–Schlichting-like waves can be excited to resonance by an external force. Although resonance will not occur for a straight channel, we conjecture that resonance will occur in the presence of an arbitrarily small (but finite) groove, with $R_c \Rightarrow 5772$ (the plane-Poiseuille-flow result) as the groove size goes to zero.

In summary, these linear-theory results indicate that a simple resonance *will* occur in grooved-channel flows forced at their (primary) natural frequency Ω_1 as the critical Reynolds number R_c is approached. The stability theory for grooved-channel flows based on Tollmien–Schlichting shear layer interaction described in I can be used to predict the frequency of the least-stable linear modes, although the response will be markedly different from that obtained in a straight channel. In the remaining sections we validate and quantify these linear-theory predictions, indicate how they are modified (but persist) when fully nonlinear effects are considered, and describe their significant effect on the transport characteristics of a flow.

4. Steady flow–heat transfer

In this section we consider the steady-state heat transfer characteristics of unmodulated ($\eta = 0$) grooved-channel flow, to provide a baseline calculation from which to evaluate the effects of oscillation on transport. The results presented are obtained by time-integration of the spectral element equivalent of equations (1)–(7) to a steady state, using meshes such as those shown in figure 7 of I. The details of our numerical methods for solution of the Navier–Stokes equations have been described and appropriately referenced in Part 1 of this paper, and will not be repeated here. The solution algorithm for the passive scalar equation (2) is very similar in nature, with the convective terms being treated with an explicit (third-order Adams–Bashforth) Galerkin-collocation scheme, and the diffusion terms being handled implicitly with standard variational projection operators. The only noteworthy subtlety associated with the passive scalar equation is that, as the boundary conditions (7) are derived from satisfaction of integral conservation laws, it is necessary that the *discrete* system also honour the appropriate integral relations. The proper conservative spectral element scheme is presented in detail in Ghaddar, Karniadakis & Patera (1986), and examples are given there of application of the method to unsteady grooved-channel flows.

With the exception of a brief study of geometric dependence in §6, all results in this paper are for the 'base' geometry, $L = 6.6666$, $l = 2.2222$, $a = 1.1111$, with periodicity index $m = 1$. (It is shown in I that the $m = 1$ steady solutions are, in fact, stable with respect to subharmonic disturbances, $m > 1$. The effect of the $m = 1$ assumption on our unsteady results will be discussed below.) In figure 3 (for figure 3c see Plate 1) we plot steady streamlines, vertical velocity 'slices', and isotherms for $R = 525$, $Pr = 1$. It is seen that, with the exception of the groove region of the flow, the thermal solution is essentially one of conduction, or, more precisely, fully developed internal flow. In the groove region of the domain the temperature
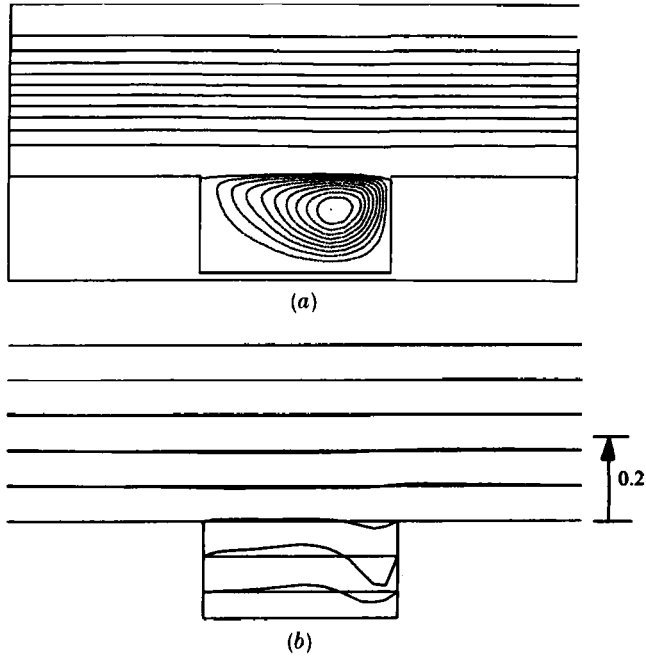
FIGURE 3. Plots of the (*a*) streamlines, and (*b*) vertical velocity slices of the steady flow in the base geometry at $R = 525$. It is seen that there is very little convective communication between the groove and channel parts of the flow.

distribution is affected by the re-circulating flow (and associated boundary layers); however the effect of the groove vortex does not extend to the channel part of the flow, as evinced by the insignificant vertical velocities above the cavity. It is clear that any transport enhancement must take the form of increased communication between the groove and channel flows.

To get an overall measure of the transport characteristics of these flows, we define a Nusselt number Nu as

$$Nu = L\left(1 + \frac{2a}{L}\right)^2 \bigg/ \int_0^{L+2a} \langle \theta - \theta_b \rangle \, ds\big|_{\partial D_\mathrm{B}}, \tag{35a}$$

where θ_b is a reference temperature taken to be the (periodic part of the) mixed-mean temperature at $x = 0$,

$$\theta_b = \left\langle \frac{3}{4} \int_{-1}^1 u(x = 0, y, t)\, \theta(x = 0, y, t) \, dy \right\rangle, \tag{35b}$$

and $\langle \ \rangle$ refers to the time average over a cycle of the flow, $t < t' < t + \Omega_\mathrm{F}^{-1}$. The Nusselt number (35) serves as a useful measure of heat transfer (our results do not change significantly for other measures of transport), and, as it involves only wall and mixed-mean temperatures, is readily determined experimentally. The geometric factors in (35a) have been chosen so as to scale the Nusselt number with average heat flux per unit length (in x); however this detail is irrelevant as regards enhancement, and is only important if comparisons are to be made between different geometries.

For the particular flow shown, the Nusselt number is $Nu = 1.12$, compared with $Nu = 1.07$ for (time-asymptotic) conduction, and $Nu = 1.35$ for the same flow in a grooveless channel. In other words, the effect of flow *is* to increase the heat transfer,

but it does not compensate for the increased 'conduction length' associated with the groove depth. In figure 4 we plot the Nusselt number as a function of Reynolds number for steady flow ($Pr = 1$), in which there is seen to be little effect of increased R. In figure 5 we plot the Nusselt number as a function of Prandtl number at $R = 525$, where, again, there is seen to be only a slight functional dependence. These two figures confirm the fact that the steady groove flow is thermally very similar to a fully developed internal flow (in which Nu is a constant, and there is no boundary-layer structure), with only a slight perturbation due to the relatively weak vortex in the groove.

5. Linear theory – numerical results

In this section we verify the conclusions of §3, and show that forcing of the linearized equations at $\Omega_F = \Omega_1$ leads to resonance and associated transport enhancement as $R \Rightarrow R_c$, that is, $\sigma_1 \Rightarrow 0$. The results are obtained by time-integration of the spectral element equivalent of (9)–(11) to a steady-periodic state, on meshes such as those in figure 7 of I. To measure the effect of oscillation on flow excitation and associated transport, we introduce two parameters: the first a pointwise amplitude parameter,

$$A(x) = \langle (v(x,t) - \langle v(x) \rangle)^2 \rangle^{\frac{1}{2}}, \tag{36}$$

corresponding to the magnitude of the fluctuating component of the vertical velocity; the second a transport enhancement parameter,

$$E = \frac{Nu(R, \eta, \Omega_F, Pr)}{Nu(R, \eta = 0, \cdot, Pr)}. \tag{37}$$

It should be noted that both A and $E-1$ are identically zero for the case of plane Poiseuille flow (i.e. no groove present, $a = 0$), as discussed in detail in §3.

In figure 6, we plot A at a point in the groove shear layer ($x = 2.963$, $y = -1.0$) as a function of Ω_F at $R = 525$ and $R = 225$, $\eta = 0.2$ (A, of course, scales linearly with η by definition). A similar plot is given in figure 7 for a point in the channel near the critical layer ($x = 0$, $y = -0.75$). It is seen that the response is precisely as expected on the basis of simple linear resonance considerations. First, the frequency response is peaked at Ω_1 calculated from linear theory (see I). Secondly, the width of the peak decreases and the magnitude increases as $R \Rightarrow R_c$ (here $R_c = 975$). Lastly, there is a secondary peak in the frequency response, due to excitation of a higher mode of the linear system Ω_k, $k > 1$. This second peak is plausibly assumed to be the second least-stable mode Ω_2, although this can not be proven on the basis of our initial-value-problem results.

In the language of I, this second mode corresponds to an $n = 1$ (one-wave) solution. Although we defer detailed flow visualizations until the discussion in §6 of nonlinear resonance, it is important in the context of linear theory to verify the wavenumber of the forced disturbances. To this end, we plot in figure 8 vertical velocity slices for the first and second modes ($\Omega_F = 0.142$ and 0.054 respectively) for the case of $R = 525$, $\eta = 0.2$. It is clear from figure 8 that the primary peak is a two-wave solution (consistent with the unforced results in I), but that the secondary peak corresponds to a one-wave mode. An important consequence of this different spatial structure is that the relative amplitude of the response in the channel as compared with that in the groove (indicative of the eigenfunction shape) is much larger for the $n = 1$ solution than for the $n = 2$ case (see figures 6 and 7). This is, no doubt, due to the fact that
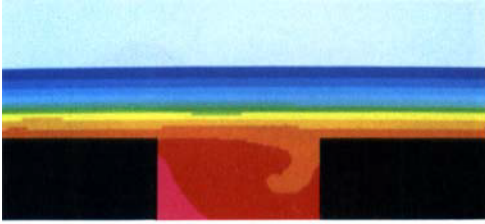
FIGURE 3 (*c*). Plot of the steady isotherms in the base geometry at $R = 525$, $Pr = 1$. The colour spectrum is used to visualize the thermal field, with red corresponding to the highest temperatures in the flow, and blue and white corresponding to the lowest temperatures (the same interpretation applies in all subsequent colour isotherm plots).
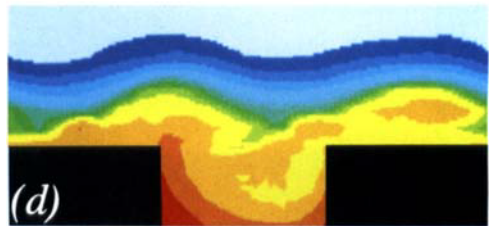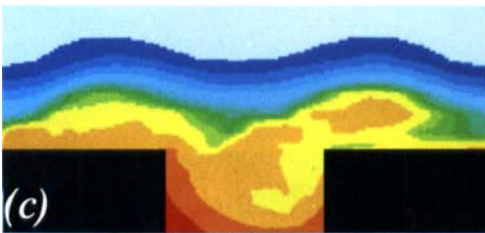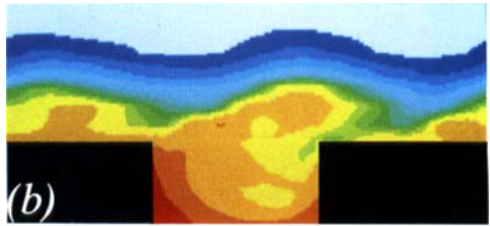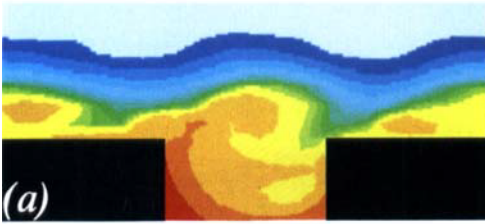
FIGURE 18. A plot of the isotherms (temperature fills) during one flow cycle in the base geometry at $R = 525$, $\eta = 0.2$, $\Omega_F = 0.168$ ($= \Omega_{n, 1}$) and $Pr = 1$. Note the imprint of the Tollmien–Schlichting waves on the resulting temperature distributions. (*a*) $\Omega_F t = 0$; (*b*) 0.2; (*c*) 0.4; (*d*) 0.6; (*e*) 0.8.
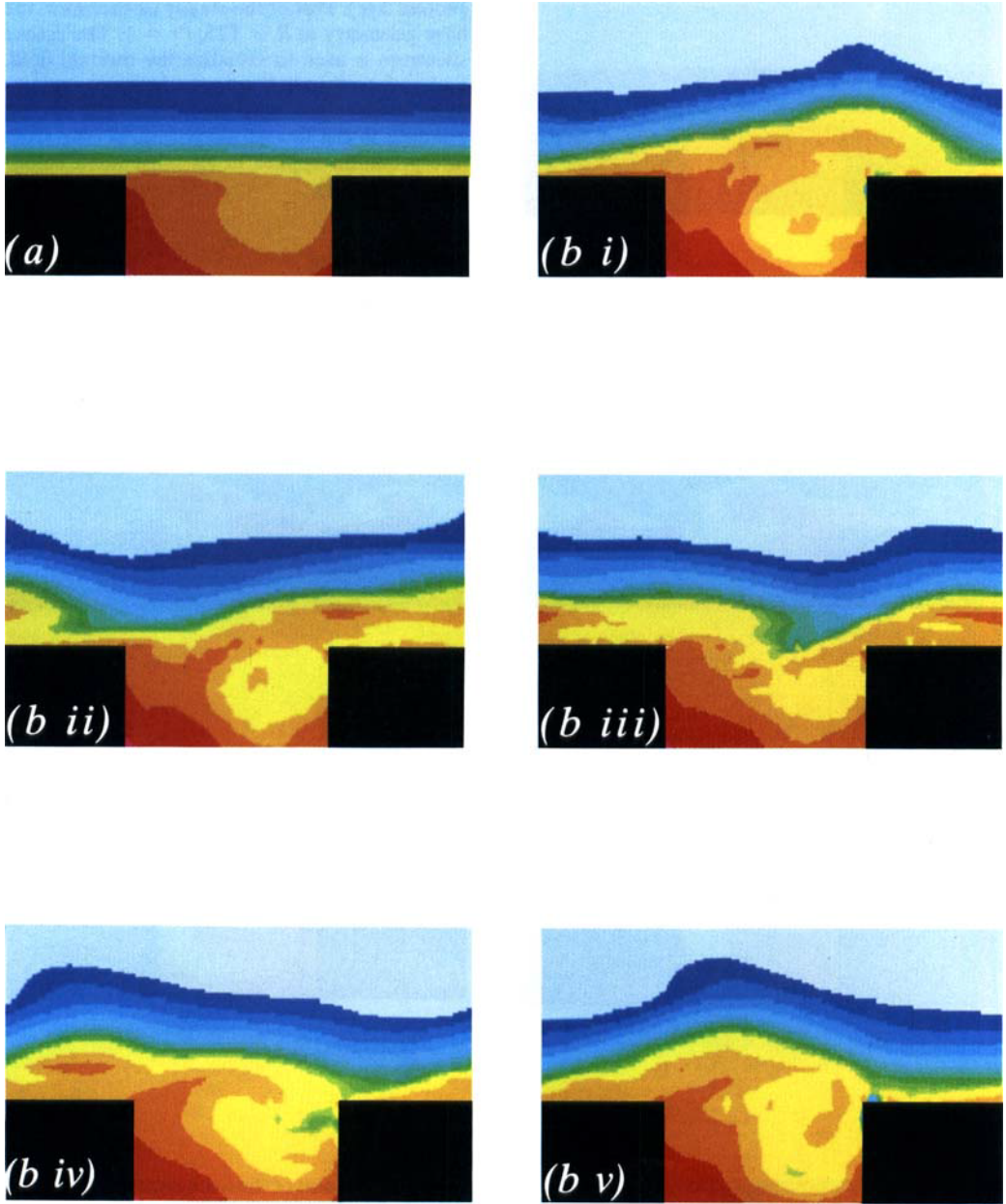
FIGURE 21. (*a*) A plot of the isotherms (temperature fills) for steady flow at $R = 525, Pr = 1$ in the shorter geometry ($L = 5.185$). (*b*) A plot of the isotherms during one flow cycle of the shorter geometry at $R = 525$, $\eta = 0.2$, $\Omega_F = 0.0925$ ($= \Omega_{n,\,1}$) and $Pr = 1$. Note the one-wave structure of the solution compared to the two-wave solutions obtained in the base geometry (see figure 18). (*i*) $\Omega_F t = 0$; (*ii*) 0.2; (*iii*) 0.4; (*iv*) 0.6; (*v*) 0.8.
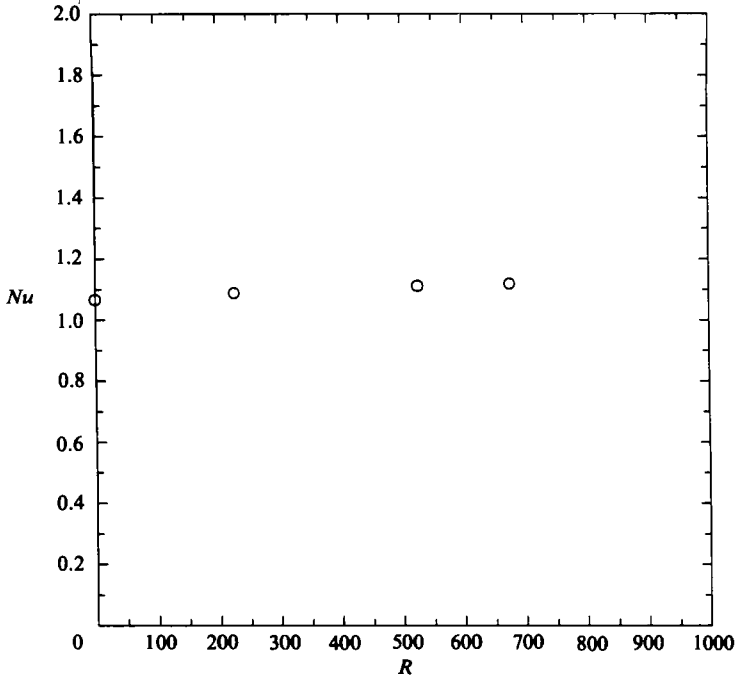
FIGURE 4. A plot of the Nusselt number as a function of Reynolds number at $Pr = 1$ for the steady flow in the base geometry. There is very little effect of increased R on Nusselt number, indicating that the steady grooved-channel flow is thermally very similar to fully developed internal flow in homogeneous geometry.
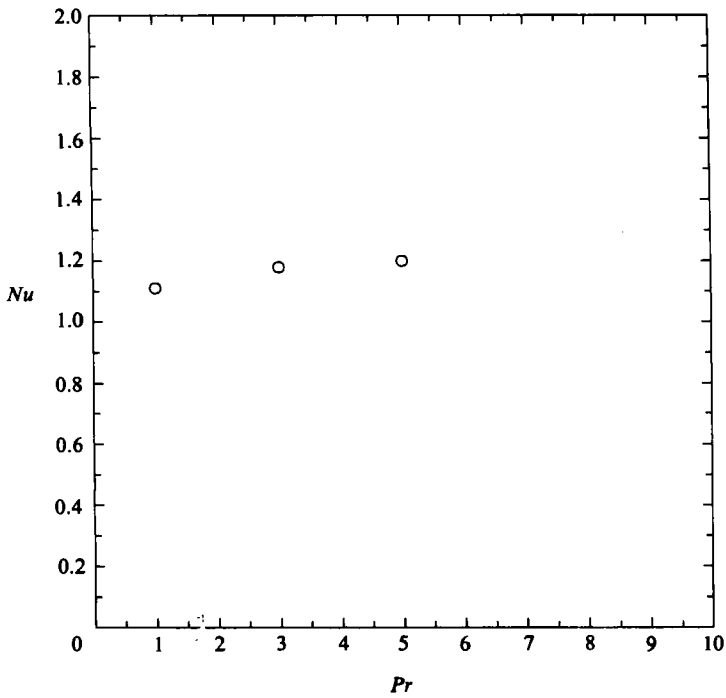
FIGURE 5. A plot of Nusselt number as a function of Prandtl number for the steady flow in the base geometry.
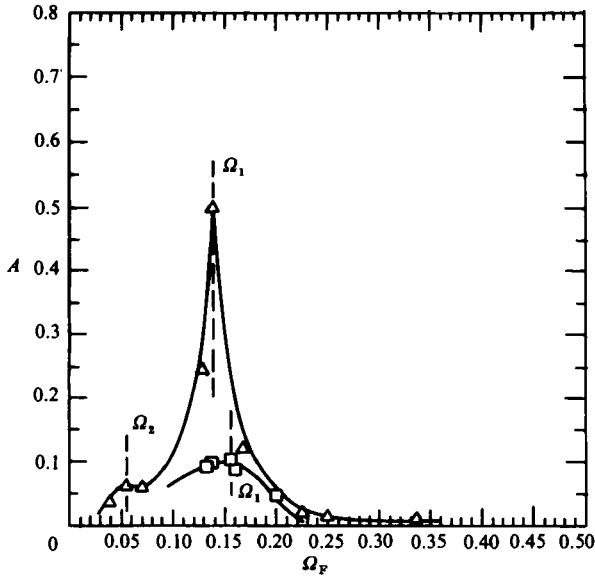
FIGURE 6. A plot of the amplitude parameter A at a point in the groove shear layer ($x = 2.963$, $y = -1$) as a function of the forcing frequency of the linearized system Ω_F at $\eta = 0.2$, for $R = 525$ ($\triangle$), and $R = 225$ ($\square$). The curves are peaked at Ω_1 calculated from linear theory. The secondary peak at Ω_2 corresponds to excitation of the second least-stable linear mode. Note the decreased amplitudes at the lower (more subcritical) Reynolds number, and the slight dependence of Ω_1 on R.
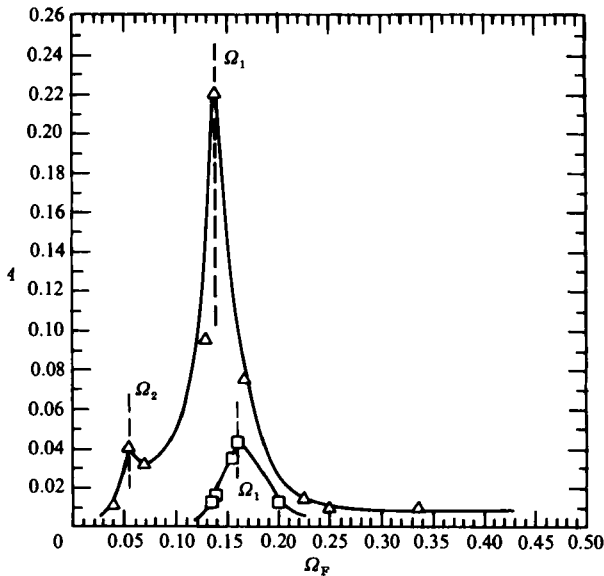
FIGURE 7. A plot of the amplitude parameter A at a point in the channel near the critical layer ($x = 0$, $y = -0.75$) as a function of the forcing frequency of the linearized system at $\eta = 0.2$ for $R = 525$ ($\triangle$), and $R = 225$ ($\square$). Note that in the channel region of the flow the secondary peak is relatively more important.

(a)

(b)
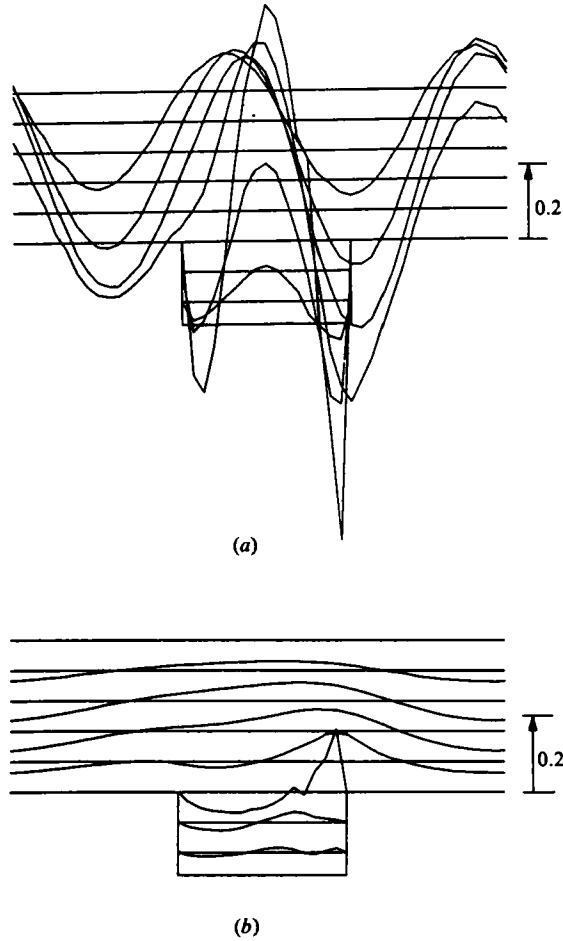
FIGURE 8. A plot of vertical velocity slices for the first and second modes of the linearized system at $R = 525$ and $\eta = 0.2$ for (a) $\Omega_F = 0.142$ $(=\Omega_1)$, and (b) $\Omega_F = 0.054$ $(=\Omega_2)$. It is clear that the primary peak is a two-wave solution, and the secondary peak is a one-wave structure.

$\alpha = 2\pi/L$ is a less stable plane-Poiseuille-flow (channel) mode than $\alpha = 4\pi/L$. We return to this point in §6 in the context of geometric dependence.

Although we were unable in I to verify our frequency theory for higher modes in our unforced direct simulations, the forced calculations presented here afford this opportunity. In particular, we note that the channel Tollmien–Schlichting theory for frequency proposed in I does extend to the second mode shown in figures 6 and 7, as $\Omega_2 = 0.054$ is in good agreement with $\Omega_{TS}(\alpha, R) = 0.055$, with $\alpha = 2\pi n/L$, $n = 1$. Despite this success for the (assumed) second mode of the system, it is clear that the frequency theory in I will not extend to arbitrarily high modes, as for sufficiently small lengthscales there will be decoupled modes for which the assumption of a shear layer/Tollmien–Schlichting compromise will no longer apply.

At this point it is appropriate to comment on the effect of the single-groove $(m = 1)$ assumption on our results. For the base geometry, it is shown in I that the steady flow is stable with respect to subharmonics $(m > 1)$, and that the least-stable mode also persists even when a larger computational domain (i.e. $m = 2$) is used. However, it is clear that for an 'infinite' number of grooves, there are an infinite number of
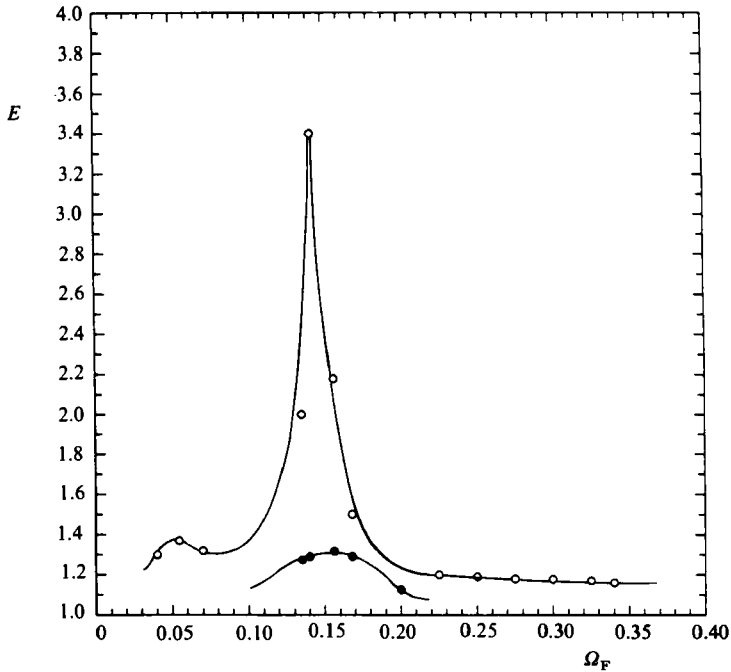
FIGURE 9. A plot of the enhancement E of the linear system as a function of Ω_F for $\eta = 0.2$, $Pr = 1$ at $R = 525$ ($\bigcirc$), and $R = 225$ ($\bullet$). The peaks in A at Ω_1 and Ω_2 translate directly into corresponding peaks in the heat-transfer enhancement.

modes corresponding to multiple-groove periodicity that are not represented in our $m = 1$ calculations, and that these modes will contribute to the forced solution. In particular, it is possible that at forcing frequencies corresponding to the frequencies of multiple-groove modes, secondary peaks will occur in the flow response that are not present in the single-groove results (e.g. figures 6 and 7). However, at least near the primary resonance ($\Omega_F = \Omega_1$), these effects should not be important given the relative stability of these higher modes compared with the critical mode; computational experiments for double-groove oscillatory forced flows confirm this conjecture.

We now investigate the effect of the resonant flow response on the transport characteristics of the flow. We plot in figure 9 the enhancement E as a function of Ω_F at $R = 525$ and 225 for $\eta = 0.2$ and $Pr = 1$. It is seen that the two peaks in A at Ω_1 and Ω_2 translate directly into peaks in the heat-transfer response, as might be expected. The reason for the enhancement is readily demonstrated by reconsidering the vertical velocity slices in figure 8; compared to the steady-flow results in figure 3, the resonant flow is characterized by large vertical velocities at the groove lip (as large as 60% of the maximum unperturbed streamwise velocity), with associated communication and mixing between the 'hot' groove and the 'cold' channel. Figure 8 also demonstrates the dramatic difference between the grooved and ungrooved (plane Poiseuille) geometry, as in the latter case there is *no* vertical velocity excitation in the context of linear theory.

Lastly, we study the effect of flow amplitude on transport enhancement E by plotting in figure 10 E as a function of η at $\Omega_F = \Omega_1$ for $R = 225$, $Pr = 1$. For small η, $E - 1 \sim O(\eta^2)$, due to the fact that the $O(\eta)$ contributions have zero time average. (It should be noted that to consistently calculate E to $O(\eta^2)$ we would have to carry
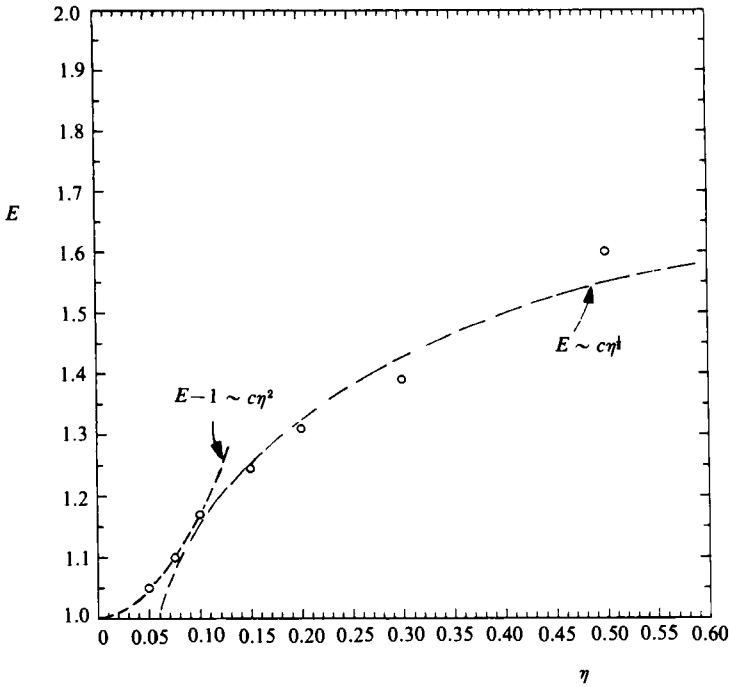
FIGURE 10. A plot of the enhancement parameter E of the linear system as a function of η at $\Omega_F = \Omega_1$ for $R = 225$, $Pr = 1$. For small η, $E - 1 \sim O(\eta^2)$, while at large η, E appears to behave as $E \sim c\eta^{\frac{1}{2}}$. The square-root dependence derives from the thermal boundary-layer structures that form as the flow excitation increases.

out (8) to the next term in the expansion. Our interest in the enhancement in the context of linear theory, however, is simply to measure the transport due to excitation of linear modes, and we have, therefore, not included these terms. Quantitative prediction of the enhancement will be given in §6, on the basis of full nonlinear calculations.) For large values of η, it appears from figure 10 that the enhancement behaves (very) approximately like $E \sim c\eta^{\frac{1}{2}}$, implying that as flow excitation increases, heat transfer is limited by spatial scales associated with thermal boundary layers. This will be discussed in greater detail in §6 in the context of Prandtl-number dependence.

6. Nonlinear resonance calculations

6.1. *Overall transport behaviour*

In this section we consider the full nonlinear response of grooved-channel flow to oscillatory perturbation, as described by (1)–(7). As before, the results are obtained by direct numerical simulation using the spectral element method, with all calculations continued until a steady-periodic solution (in v and θ) is achieved.

To begin, in figure 11 we plot A at the point in the groove shear layer as a function of Ω_F at $R = 525$ and 225, $\eta = 0.2$, analogous to figure 6 for linear theory. In figure 12 we present the same results for a point in the channel near the critical layer of the travelling wave. We note several effects due to nonlinearity. First, the frequencies at which A achieves maxima $\Omega_{n,1}$, $\Omega_{n,2}$ ('nonlinear' natural frequencies), are shifted from their linear counterparts Ω_1, Ω_2 respectively. The effect is most pronounced for
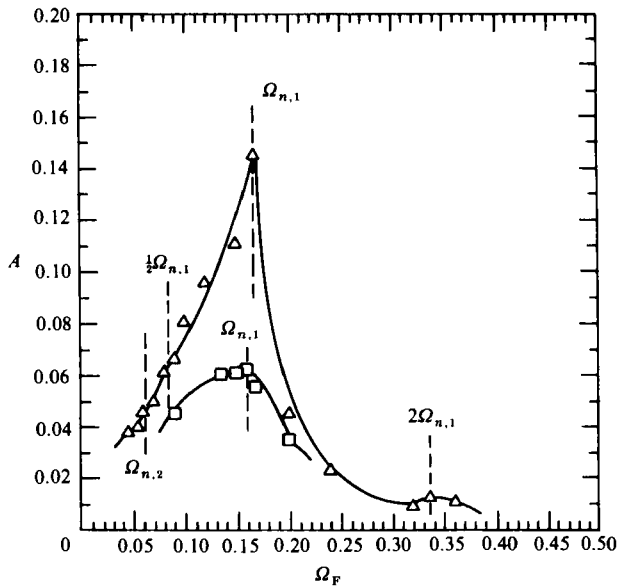
FIGURE 11. A plot of the amplitude parameter A at a point in the groove shear layer ($x = 2.963$, $y = -1$) as a function of the forcing frequency Ω_F of the nonlinear system at $\eta = 0.2$ for $R = 525$ ($\triangle$), and $R = 225$ ($\square$). The optimal frequency for maximum enhancement, $\Omega_{n,1}$, is slightly shifted from Ω_1 predicted by linear theory.
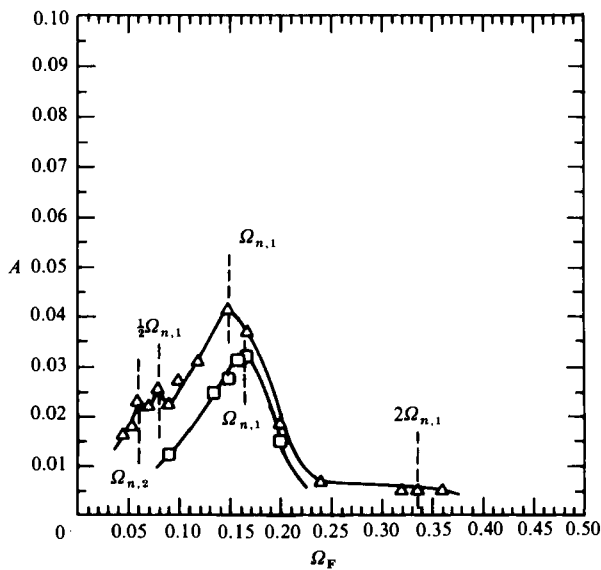
FIGURE 12. A plot of the amplitude parameter A at a point in the channel near the critical layer ($x = 0$, $y = -0.75$) as a function of the forcing frequency of the nonlinear system at $\eta = 0.2$, for $R = 525$ ($\triangle$), and $R = 225$ ($\square$). Peaks or inflexions appear at $\Omega_{n,1}$, $\Omega_{n,2}$, $\frac{1}{2}\Omega_{n,1}$ and $2\Omega_{n,1}$ in both this figure and figure 11.
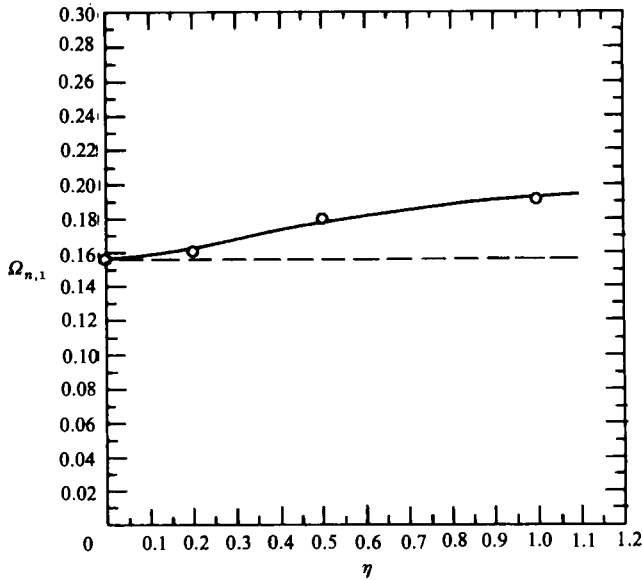
FIGURE 13. A plot of $\Omega_{n,1}$ as a function of η at $R = 225$ for the nonlinear system. The frequency shift for maximum enhancement increases as the flow modulation is increased.

Ω_1 and $R = 525$, as the amplitudes are larger for the first mode and the higher Reynolds number, and hence the nonlinear effects are more important. Secondly, the amplitudes of the peaks are reduced compared with the linear case, figures 6 and 7, corresponding to increasing nonlinear attenuation (saturation) as $R \Rightarrow R_c$. Note again that the primary peak at high Reynolds number is most seriously affected. Thirdly, we see the appearance of new peaks at $\frac{1}{2}\Omega_{n,1}$ and $2\Omega_{n,1}$, corresponding to excitation of sub- and superharmonics. As in the linear case, the one-wave peaks are more pronounced in the channel part of the domain.

It can be seen from comparison of figures 11 and 12 that $\Omega_{n,1}$ does not appear to be precisely the same at all points in the flow domain; this is due to (spatially dependent) contamination of the resonant mode by the higher modes of the system. Although this effect is most pronounced for the nonlinear calculations reported here, even within the context of linear theory the peaks in the amplitude response need not be uniformly at $\Omega_F = \Omega_1$, except in the limit that $R \Rightarrow R_c$. As this frequency shift is quite small for the range of parameters studied, we continue to speak of a single 'optimal' frequency as regards both amplitude and enhancement.

The main conclusion based on comparison of figures 11 and 12 with figures 6 and 7 is that the resonance phenomenon presented here is essentially linear in nature, with nonlinearity having a significant quantitative, but not qualitative, effect. As expected, the nonlinear modifications become more important at larger flow amplitudes, whether these large amplitudes are due to increased forcing amplitude η, or to operation at near-resonant conditions (Ghaddar 1985). As an example of the magnitude of these effects, in figure 13 we plot $\Omega_{n,1}$ vs. η for $R = 225$, where it is seen that a 30% shift in 'optimal' frequency occurs as η varies between 0 and 1.0. Note that, as $\eta \Rightarrow 0$, $\Omega_{n,1}$ approaches the linear result Ω_1, as must be the case.

Considering now the transport enhancement resulting from the full nonlinear calculation, we present in figure 14 E as a function of Ω_F for $R = 525$ and 225 at $\eta = 0.2$, $Pr = 1$, analogous to the linear results given in figure 9. We see basically all
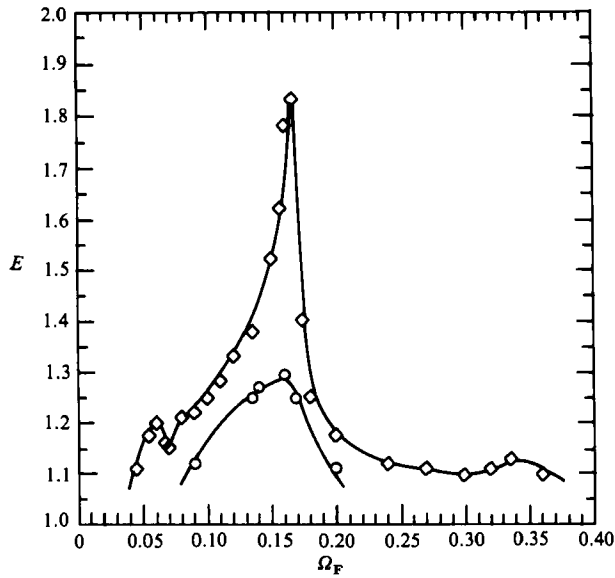
FIGURE 14. A plot of the enhancement E as a function of Ω_F of the nonlinear system at $\eta = 0.2$, $Pr = 1$ for $R = 525$ ($\Diamond$), and $R = 225$ ($\bigcirc$). The peaks in A (see figures 11 and 12) translate directly into peaks in the heat-transfer enhancement.

the same nonlinear effects as in A, with frequency shifts, amplitude attenuation, and appearance of primary frequency multiples. Note that the peak enhancement at $R = 525$ is $E = 1.83$, a significant augmentation of heat transfer for an amplitude modulation as small as $\eta = 0.2$. Again comparing this with the case of a straight channel, in which there would be no enhancement at this Reynolds number, we see the significant effect of the groove on flow response.

6.2. Flow visualization

In order to better see the physical mixing processes responsible for transport enhancement in oscillatory grooved-channel flows, we consider here visualizations of the instantaneous velocity and temperature fields during the flow cycle. In figures 15, 16, 17, and 18 we plot the instantaneous streamlines, vertical velocity slices, vorticity contours, and isotherms (temperature fills) respectively, during a full cycle for $R = 525$, $\Omega_F = \Omega_{n,1}$, $\eta = 0.2$, $Pr = 1$. First, all the pictures indicate significant mixing between the groove and bulk flow. This is seen in figure 15 by the bulging of the groove vortex into the channel, and in figure 16 by the large vertical velocities at the groove lip. Even more dramatically, we see in figure 18 (plate 1) the motion of packets of 'hot' fluid into the channel from the groove, and the motion of packets of 'cold' fluid from the channel into the groove.

Secondly, it is clear that the solution is, indeed, an $n = 2$ (two-wave) channel mode, as would be expected from the linear theory results of I. This can be seen particularly well in the isotherm pictures in figure 18, in which the two-wave travelling-wave solution in the channel is clearly delineated; figure 18 is, in essence, a thermal visualization of Tollmien–Schlichting waves. Note that the form of the Tollmien–Schlichting wave, together with the fact that the temperature is approximately material in the interior of the domain, forces on the thermal solution the appearance of two alternate hot and cold spots per periodicity length, with the hot spots at the
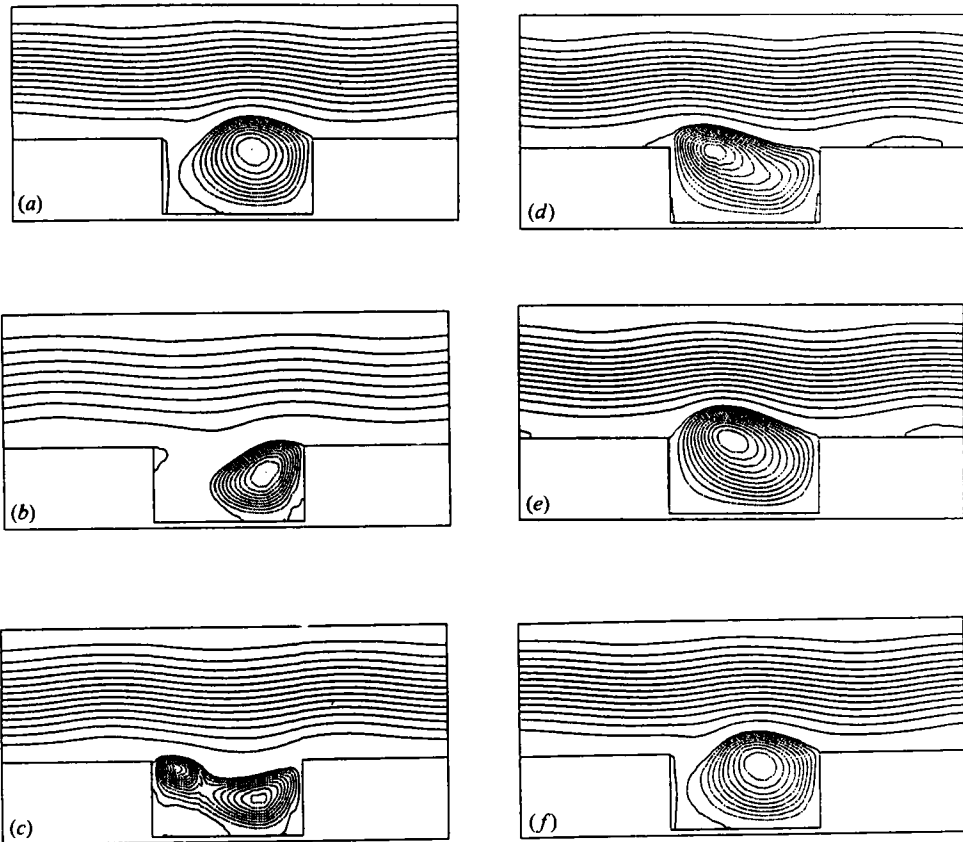
FIGURE 15. A plot of the instantaneous streamlines during the flow cycle at $R = 525$, $\eta = 0.2$, $\Omega_F = 0.168$ ($= \Omega_{n,1}$) for the base geometry. The groove vortex is seen to bulge out into the channel flow during the course of the cycle. (a) $\Omega_F t = 0$; (b) 0.2; (c) 0.4; (d) 0.6; (e) 0.8; (f) 1.0.

wave 'crests', and the cold spots at the wave 'troughs'. In essence, as a wave trough passes over the groove, it forces cold fluid into the downstream side of the cavity, which in turn pushes hot fluid from the upstream part of the groove into the associated oncoming wave crest. It is clear from figure 18 that spatial 'compatibility' between the groove and channel flows (as enforced by the choice of n, the number of channel waves per periodicity length) is critical to effective transport.

Although the central focus of the current paper is on the effect of resonance on heat-transfer enhancement, it is clear that subcritical resonance will also have a significant effect on the transition process in grooved-channel flows. In I, it is shown that supercritical grooved-channel flows closely resemble the secondary flows (finite-amplitude Tollmien–Schlichting waves) seen in plane Poiseuille flow (Orszag & Patera 1983); figures 15–18 demonstrate that this similarity extends to forced subcritical grooved-channel flows. This suggests that the three-dimensional secondary instability isolated in plane channels may play an important role in transition in grooved-channel flows not only at supercritical Reynolds numbers, but also at subcritical Reynolds numbers. In particular, the extreme sensitivity of grooved-channel flows to external disturbances, as evidenced by subcritical resonance, could well lead to transition for Reynolds numbers less than R_c (≈ 975 for the base geometry); small external perturbations are amplified into relatively large-amplitude Tollmien–Schlichting
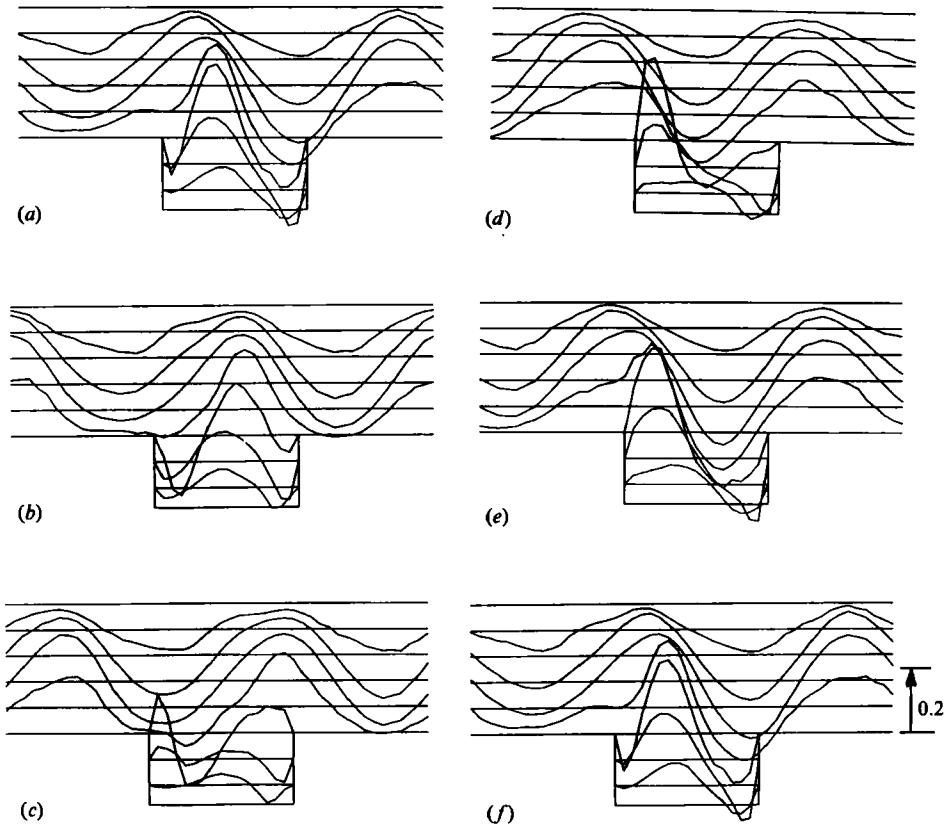
FIGURE 16. A plot of the instantaneous vertical velocity slices during the flow cycle at $R = 525$, $\eta = 0.2$, $\Omega_F = 0.168$ $(=\Omega_{n,1})$ in the base geometry. Note the large vertical velocities at the groove lip, as well as the two-wave structure per periodicity length in the channel region. (a) $\Omega_F t = 0$; (b) 0.2; (c) 0.4; (d) 0.6; (e) 0.8; (f) 1.0.

waves, which may then, in turn, become unstable to three-dimensional instabilities. The increased receptivity of grooved-channel flows is, no doubt, at least partially responsible for the relative instability of general rough-walled systems as compared to their planar counterparts.

6.3. *Prandtl-number dependence*

The dependence of the enhancement E on the flow amplitude η for the linear calculations in §5 suggests that for large convective motions the heat transfer is limited by thermal boundary layers at the grooved wall. In this section we verify this conjecture by considering the Prandtl-number dependence of the enhancement.

It is clear from figure 5 in §4 that the dependence of the steady Nusselt number on Prandtl number is very weak, owing to the fact that steady grooved-channel flow is only slightly different from fully developed flow in a straight channel. To use this same dependence in predicting the effect of Prandtl number on resonant flows is not correct, however, as for large convective motions we expect boundary layers to form, in which the transport now does depend on the velocity and relative diffusivities.

In particular, if we assume that for large enhancement the flow approaches a state
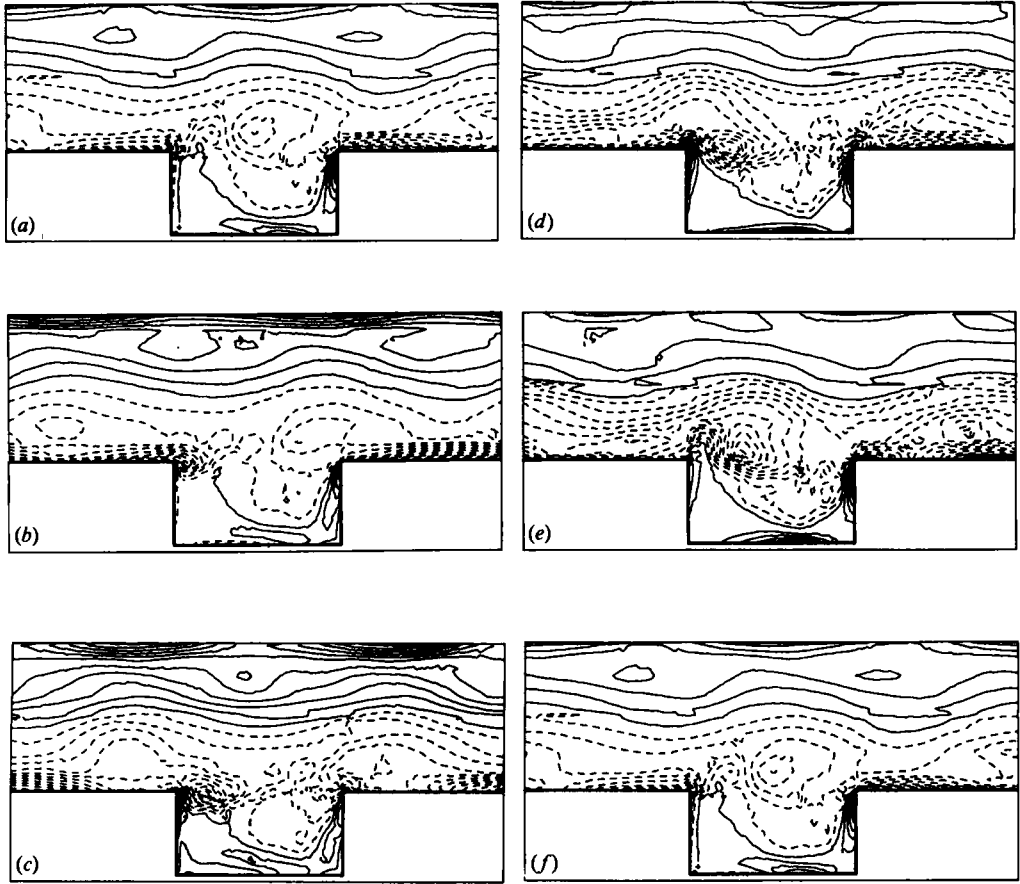
FIGURE 17. A plot of the vorticity contours during the flow cycle at $R = 525$, $\eta = 0.2$, $\Omega_{\mathrm{F}} = 0.168$ ($=\Omega_{n,1}$) in the base geometry. Note the significant vorticity generation at the upstream groove edge. (a) $\Omega_{\mathrm{F}} t = 0$; (b) 0.2; (c) 0.4; (d) 0.6; (e) 0.8; (f) 1.0.

of outer convectively dominated regions matched to thin thermal boundary layers at walls, this suggests the scaling

$$Nu(R, \eta, \Omega_{\mathrm{F}}, Pr) = Nu'(R, \eta, \Omega_{\mathrm{F}}) Pr^{\kappa}, \tag{38a}$$

$$\kappa \Rightarrow \tfrac{1}{3}, \quad E' \Rightarrow \infty, \tag{38b}$$

for $Pr > 1$, the $\frac{1}{3}$-power motivated by the similarity solution for high-Prandtl-number flat-plate boundary-layer flow (Schlichting 1955). Here E' is the reference enhancement at $Pr = 1$, $E'(R, \eta, \Omega_{\mathrm{F}}) = E(R, \eta, \Omega_{\mathrm{F}}, Pr = 1)$. We demonstrate that (38) is, indeed, the case, by plotting κ vs. $E' - 1$ in figure 19, where it is seen that κ does appear to approach $\frac{1}{3}$ as $E' \Rightarrow \infty$. The data in figure 19 derive from a number of runs with different frequency, Reynolds number, and amplitude, with Prandtl numbers in the range $1 < Pr < 5$. (The calculations are, of course, increasingly difficult as the Prandtl number increases, due to the presence of very thin thermal boundary layers.) As regards enhancement, figure 19 also implies that $E \sim Pr^{\frac{1}{3}}$ for large E', as the Nusselt number for the steady flow has virtually no Prandtl number dependence (see figure 5).
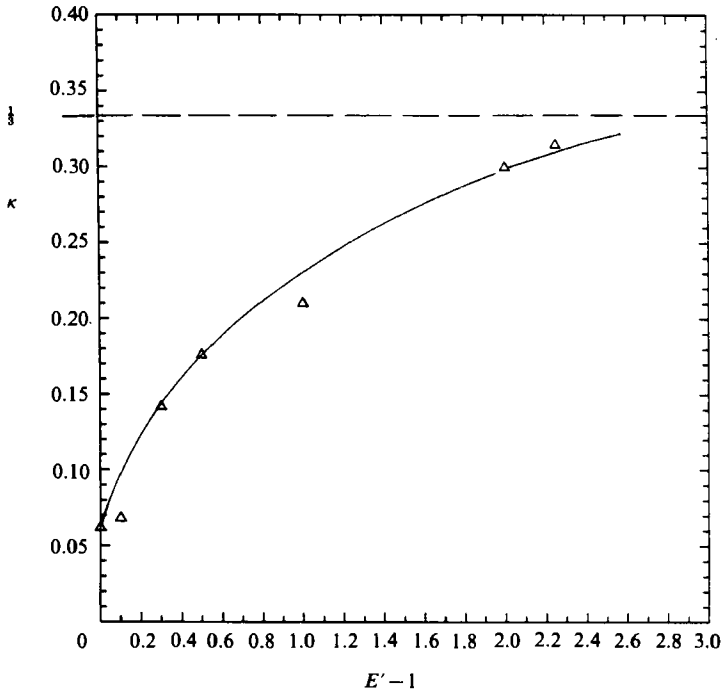
FIGURE 19. A plot of Prandtl-number power dependence κ as a function of $E' - 1$. Note κ approaches $\frac{1}{3}$ as $E' \Rightarrow \infty$, as expected from simple boundary-layer estimates.

6.4. Geometric dependence

In I, we presented a general theory for prediction of the natural frequency of (open-cavity) grooved-channel flows based on the dispersion relation for Tollmien–Schlichting channel waves, and demonstrated the accuracy of the theory over a wide range of geometric parameters. This theory, in conjunction with the resonance results presented in the current paper, allows for *a priori* prediction of the optimal frequency for transport enhancement for any given geometric configuration.

As an example of the general validity of this approach, as well as a demonstration of the complex interaction between flow amplitude, geometry, and optimal enhancement, we consider here a new geometry for which the *primary* frequency Ω_1 corresponds to a one-wave ($n = 1$) solution. The particular geometry chosen has parameters $L = 5.185$, $l = 2.2222$, $a = 1.1111$, representing a slightly shorter configuration than the base case, for which $L = 6.6666$. In figure 20 we plot E as a function of Ω_F at $R = 525$, $\eta = 0.2$, $Pr = 1$ for this shorter domain. It is seen that, as expected, peak enhancement occurs at a frequency only slightly (nonlinearly) shifted from the linear result of $\Omega_1 = 0.083$. In figure 21 (plate 2) we show the isotherms (temperature fills) during one cycle for the shorter geometry, demonstrating the one-wave nature of the flow and temperature distribution.

We make two points by way of comparison of figures 20 and 21 with the corresponding curves for the base geometry (figures 14 and 18 respectively). First, the shorter geometry is, in fact, less stable than the base geometry (see I), from which it follows that the resonant flow excitation (e.g. A) will be greater; this can be seen by the significant wave distortion in figure 21 compared to that in figure 18. However, as has been shown in the context of both linear and nonlinear theory, one-wave
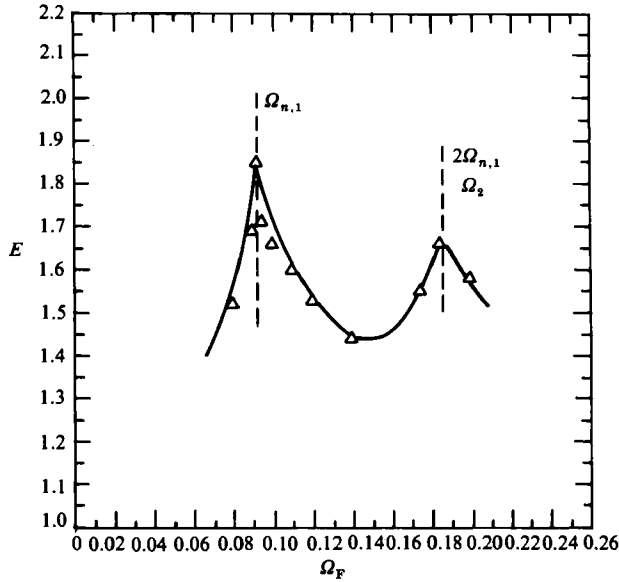
FIGURE 20. A plot of the enhancement E as a function of Ω_F, for the shorter-periodicity-length geometry, at $R = 525$, $\eta = 0.2$, and $Pr = 1$. The peak in the enhancement occurs at $\Omega_{n,1}$, slightly shifted from Ω_1 of the linear system. A strong secondary peak also occurs at $\Omega_F = 2\Omega_{n,1}$ ($\approx \Omega_2$).

solutions for these geometries are more 'channel' dominated than their two-wave counterparts, and as a result the increase in flow amplitude in the groove (compared to the base geometry at optimal conditions) is minimal. This is, no doubt, the primary reason why this less stable (shorter) geometry results in only a negligible increase in peak enhancement over the base case, as the critical 'hot' points in the flow (e.g. the groove) are not favoured by the eigenfunction shape of the one-wave excited mode. Another possible cause for the somewhat disappointing enhancement is that the one-wave solution in the channel is less convoluted than the corresponding two-wave mode, resulting in increased cross-stream thermal resistance and hence lower Nusselt numbers. In summary, resonant transport enhancement is not only a question of flow magnitude, but also proper velocity–temperature correlation.

The second point concerns the secondary peak in figure 20, which is seen to be significantly larger than any secondary peaks that appeared in the base geometry. We conjecture that this is due to the coincidence that for this particular geometry, Reynolds number, and amplitude, $2\Omega_{n,1}$ ($=0.185$) is the same as Ω_2 ($\approx \Omega_{TS}(\alpha = 4\pi/L, R) = 0.184$) to within 0.4% (for the base geometry $\frac{1}{2}\Omega_{n,1}$ differs from Ω_2 by approximately 30%). Consequently, there is a 'secondary' resonance between the nonlinear and linear modes, which results in significant flow excitation and transport enhancement. To verify the validity of this claim would require a more complete analysis of the nonlinear and linear response of this shorter geometry. Note that another instance in which we expect to see a 'broad' (bi-modal) frequency response is for geometries at or close to the transition point at which the relative stability of the one- and two-wave solutions changes.

These results for the shorter geometry highlight some of the difficulties associated with practical implementation of subcritical resonance. In addition to the impediments associated with the narrow peaks and nonlinear sensitivity of the frequency response, figure 20 demonstrates the large effect geometry can have on optimal conditions, with

jump changes in frequency occurring for only slight changes in domain shape (see figure 18 of I). It follows that enhancement by resonance in practical applications is potentially 'ill posed', success relying heavily on detailed information on the parameters and operating conditions of the system. Furthermore, application of resonant enhancement to practical devices must consider the penalties as well as benefits associated with large flow excitation, such as increased dissipation and pressure drop, and make appropriate comparisons with competing augmentation schemes (e.g. turbulence). Although preliminary results indicate a lesser proportional increase in dissipation than heat transport at optimal conditions (Ghaddar 1985), the viability of modulatory perturbation will certainly be context-dependent.

The same phenomena that make application of subcritical resonance a delicate matter, also make experimental confirmation a non-trivial task. A series of companion experiments is currently underway (Greiner *et al.* 1986), the first results of which are in good agreement with the theoretical and numerical results presented here for the resonance phenomenon, the Orr–Sommerfeld frequency theory, the spatial structure of the flow, and the significant transport enhancement associated with resonant flow excitation. Furthermore, experiments at high Reynolds numbers (Greiner 1986) indicate that resonant excitation may, indeed, extend to turbulent flows, consistent with earlier work (Townes & Sabersky 1966) that implicated periodic groove bursts as being critical in rough-wall turbulent transport.

The most serious assumption of the numerical investigation reported here is that of two-dimensionality. Future work will address the degree to which the resonance phenomenon discussed here is modified by, and extends to, three-dimensional flow, using both three-dimensional (spanwise) Fourier analysis of two-dimensional grooves (Ghaddar & Patera 1986), and full three-dimensional spectral element simulation of grooves and protuberances with spanwise geometric variation (Karniadakis, Bullister & Patera 1986). Although the details of the frequency selection process will certainly be modified for these more-complicated situations, there is little doubt that the phenomenon of subcritical resonance is not restricted to the particular geometries presented here, and should obtain in a wide class of flows in non-homogeneous domains.

REFERENCES

ARVIZU, D. E. & MOFFAT, R. J. 1982 Experimental heat transfer from an array of heated cubical elements on an adiabatic channel wall. *Rep. No.* HMT-33, Thermosciences Div. Stanford University, Stanford, California.

ASHIWAKE, N., NAKAYAMA, W., DAIKOKU, T. & KOBAYASHI, F. 1983 Forced convective heat transfer from LSI packages in an air-cooled wiring card array. In *Heat Transfer in Electronic Equipment* (ed. S. Oktay & A. Bar-Cohen), HTD-28, p. 35. ASME.

BELLHOUSE, B. J., BELLHOUSE, F. H., CURL, C. M., MACMILLAN, T. I., GUNNING, A. J., SPRATT, E. H., MACMURRAY, S. B. & NELEMS, J. M. 1973 A high efficiency membrane oxygenator and pulsatile pumping system, and its application to animal trials. *Trans. Am. Soc. Artif. Int. Organs* **19**, 77.

DAVIS, S. H. 1976 The stability of time periodic flows. *Ann. Rev. Fluid Mech.* **8**, 57.

DIPRIMA, R. C. & HABETLER, G. J. 1969 A completeness theorem for non-selfadjoint eigenvalue problems in hydrodynamic stability. *Arc. Rat. Mech. Anal.* **34**, 218.

DRAZIN, P. G. & REID, W. H. 1981 *Hydrodynamic Stability.* Cambridge University Press.

GHADDAR, N. K. 1985 Numerical investigation of heat transfer enhancement due to oscillatory flow over furrowed walls. Ph.D. thesis, M.I.T., Cambridge, Massachusetts.

GHADDAR, N. K., KARNIADAKIS, G. E. & PATERA, A. T. 1986 A conservative isoparametric spectral element method for forced convection; application to fully-developed flow in periodic geometries. *Numer. Heat Transfer* **9**, 277.

GHADDAR, N. K., KORCZAK, K. Z., MIKIC, B. B. & PATERA, A. T. 1986 Numerical investigation of incompressible flow in grooved channels. Part 1. Stability and self-sustained oscillations. *J. Fluid Mech.* **163**, 99.

GHADDAR, N. K. & PATERA, A. T. 1986 Stability and resonance in grooved-channel flows. In *Proc. ICASE/Nasa–Langley Workshop on Stability of Time Dependent and Spatially Varying Flows, Hampton, Virginia* (to appear).

GHADDAR, N. K., PATERA, A. T. & MIKIC, B. B. 1984 Heat transfer enhancement in oscillatory flow in a grooved channel. *AIAA Paper No.* 84-0495.

GREINER, M. 1986 Experimental investigation of resonance and heat transfer enhancement in grooved channels. Ph.D. thesis, M.I.T., Cambridge, Massachusetts.

GREINER, M., GHADDAR, N. K., MIKIC, B. B. & PATERA, A. T. 1986 Resonant convective heat transfer in grooved channels. In *Proc. 8th Intl Heat Transfer Conf., San Francisco* (to appear).

JOSHI, C. H., KAMM, R. D., DRAZEN, J. M. & SLUTSKY, A. S. 1983 An experimental study of gas exchange in laminar oscillatory flow. *J. Fluid Mech.* **133**, 245.

KARNIADAKIS, G. E., BULLISTER, E. T. & PATERA, A. T. 1986 A spectral element method for solution of the two- and three-dimensional time-dependent incompressible Navier–Stokes equations. In *Proc. Europe–USA Symp. on Finite Element Methods for Nonlinear Problems, Norway.* Springer (to appear).

KAYS, W. M. & LONDON, A. L. 1955 *Compact Heat Exchangers.* McGraw-Hill.

KERN, D. Q. & KRAUS, A. D. 1972 *Extended Surface Heat Transfer.* McGraw-Hill.

MAGEN, M. & PATERA, A. T. 1986 Resonance conditions for forced two-dimensional channel flows. In *Proc. SIAM Conf. on Mathematics Applied to Fluid Mechanics and Stability, dedicated to Richard C. DiPrima, RPI* (to appear).

ORSZAG, S. A. & PATERA, A. T. 1983 Secondary instability of wall-bounded shear flows. *J. Fluid Mech.* **128**, 347.

SCHLICHTING, H. 1955 *Boundary Layer Theory.* McGraw-Hill.

SOBEY, I. J. 1980 On flow through furrowed channels. Part 1: Calculated flow patterns. *J. Fluid Mech.* **96**, 7.

SOBEY, I. J. 1982 Oscillatory flows at intermediate Strouhal number in asymmetric channels. *J. Fluid Mech.* **125**, 359.

SOBEY, I. J. 1983 The occurrence of separation in oscillatory flow. *J. Fluid Mech.* **134**, 247.

STEPHANOFF, K. D., SOBEY, I. J. & BELLHOUSE, B. J. 1980 On flow through furrowed channels. Part 2: Observed flow patterns. *J. Fluid Mech.* **96**, 27.

TOWNES, H. W. & SABERSKY, R. H. 1966 Experiments on the flow over a rough surface. *Intl J. Heat Mass Transfer* **9**, 729.

WATSON, E. J. 1983 Diffusion in oscillatory pipe flow. *J. Fluid Mech.* **133**, 233.